# Stochastic pre-event preparation for enhancing resilience of distribution systems

Qianzhi Zhang [a],[*], Zhaoyu Wang [a], Shanshan Ma [b], Anmar Arif [c]

[a] *Department of Electrical and Computer Engineering, Iowa State University, Ames, IA 50011, USA*
[b] *School of Electrical, Computer and Energy Engineering, Arizona State University, Tempe, AZ 85287, USA*
[c] *Department of Electrical Engineering, King Saud University, Riyadh 11451, Saudi Arabia*

## ARTICLE INFO

## ABSTRACT

Extreme weather events are the common causes for power supply interruptions and power outages in electrical distribution systems. Improving the distribution system and enhancing its resilience is becoming crucial due to the increased frequency of extreme weather events. Preparation and allocation of multiple flexible resources, such as mobile resources, fuel resources, and labor resources before extreme weather events can mitigate the effects of extreme weather events and enhance the resilience of power distribution systems. In this paper, a two-stage stochastic mixed-integer linear programming (SMILP) is proposed to optimize the preparation and resource allocation process for upcoming extreme weather events, which leads to faster and more efficient post-event restoration. The objective of the proposed two-stage SMILP is to maximize the served load and minimize the operating cost of flexible resources. The first stage in the optimization problem selects the amounts and locations of different resources. The second stage considers the operational constraints of the distribution system and repair crew scheduling constraints. The proposed stochastic pre-event preparation model is solved by a scenario decomposition method, Progressive Hedging (PH), to ease the computational complexity introduced by a large number of scenarios. Furthermore, to show the impact of solar photovoltaic (PV) generation on system resilience, three types of PV systems are considered during a power outage and the resilience improvements with different PV penetration levels are compared. Numerical results from simulations on a large-scale (more than 10,000 nodes) distribution feeder have been used to validate the effectiveness and scalability of the proposed method.

## 1. Introduction

In recent years, the relationship between climate change, extreme weather events, and power outages have become the focus of discussion worldwide [1,2]. The aging infrastructure of the electric grid combined with the increase in severe weather events have highlighted the harsh reality of how vulnerable the distribution grid is. For example, high temperatures from heatwaves will limit the amount of energy that can be transferred [3], lightning strikes cause faults on the lines [4], and the high winds from storms may damage overhead lines [5]. In the U.S., extreme weather events have caused 50% to 60% of the power interruptions [6] and $20 to $55 billion annual economic losses [7]. To mitigate the impacts of extreme weather events on electric infrastructures and power grids, extensive efforts have been devoted toward proposing the concept of *resilience*. In [8], resilience was defined as a property of systems representing their response to and recovery from low probability and high impact events. The measurements of system resilience are disciplined into ecological resilience [9], psychological resilience [10], risk management [11], and energy security [12].

About 90% of weather-related power interruptions and outages are led by failures in distribution systems [13]. Various resilience-enhancing strategies have been studied in distribution systems [14], such as the long-term planning, the pre-event preparation, and the post-event restoration. The long-term planning provides utility companies the actionable resilience-enhanced methods to upgrade infrastructures in the long-term [15]. For example, the optimal line hardening strategies against extreme weather-related hazards are developed to physically improve electric infrastructure and enhance the long-term resilience of the distribution system in [16–19]. The post-event restoration is used by utility companies to prioritize service restoration efforts, schedule repair crews and manage network reconfiguration after the extreme weather events [20]. For example, the dynamic formation of microgrids (MGs) and optimal coordination between multiple MGs are

---

* Corresponding author.
*E-mail addresses:* qianzhi@iastate.edu (Q. Zhang), wzy@iastate.edu (Z. Wang), shansh19@asu.edu (S. Ma), anarif@ksu.edu.sa (A. Arif).

**Notations**

**List of abbreviations**

| | |
|---|---|
| CI | Confidence interval |
| DERs | Distributed energy resources |
| DGs | Distributed generators |
| EF | Extensive form |
| ESS | Energy storage system |
| MEGs | Mobile emergency generators |
| MESs | Mobile storage devices |
| MRP | Multiple replication procedure |
| PH | Progressive hedging |
| PV | Photovoltaic generation |
| SOC | State of charge |
| SMILP | Stochastic mixed-integer linear programming |

**Indexes**

| | |
|---|---|
| $c$ | Index of conductor between poles |
| $i, j$ | Index of bus |
| $ij$ | Index of line between bus $i$ and bus $j$ |
| $k$ | Index of conductor or line |
| $l$ | Index of network loop |
| $p$ | Index of pole |
| $s$ | Index of scenario |
| $t$ | Index of time instant |

**Sets**

| | |
|---|---|
| $\Omega_B$ | Set of line switches |
| $\Omega_{CN}$ | Set of candidate buses for MEGs and MESs |
| $\Omega_{DL}$ | Set of damaged lines |
| $\Omega_{EG}$ | Set of buses that have fuel-based emergency generators |
| $\Omega_{ES}$ | Set of buses with ESSs |
| $\Omega_{ESC}$ | Set of buses with all types of storage units |
| $\Omega_G$ | Set of generators |
| $\Omega_K$ | Set of lines |
| $\Omega_{loop}$ | Set of network loops |
| $\Omega_N$ | Set of buses |
| $\Omega_R$ | Set of network regions |
| $\Omega_{PV}$ | Set of PV systems |
| $\Omega_{PV}^G$ | Set of grid-following PV systems |
| $\Omega_{PV}^H$ | Set of hybrid on-grid/off-grid PV systems |
| $\Omega_{PV}^C$ | Set of grid-forming PV systems |

**Parameters**

| | |
|---|---|
| $a, b_s$ | Coefficients associated with the compact first stage variable $x$ and compact second stage variable $y_s$ |
| $C^F$ | Unit cost of fuel consumption of generators (L/kWh) |
| $C^{SW}$ | Unit cost of line switches ($) |
| $C_i^D$ | Unit cost of load shedding ($/kWh) |
| $d_{i,\phi,t}^p$ | Active power demand of bus $i$, phase $\phi$ and time $t$ |
| $E_i^{Cap}$ | Maximum capacity of ESSs of bus $i$ |

| | |
|---|---|
| $E_i^{SOC,max}, E_i^{SOC,min}$ | Maximum and minimum permissible range of SOC of bus $i$ |
| $P_i^{Ch,max}, P_i^{Dis,max}$ | Maximum charging and discharging powers of ESS of bus $i$ |
| $P_k^{K,max}, Q_k^{K,max}$ | Active and reactive power flow limits |
| $P_i^{G,max}, Q_i^{G,max}$ | Active/reactive power output limits of generator |
| $P_{i,\phi,t,s}^{PV}$ | Active power output of PV systems of bus $i$, phase $\phi$, time $t$ and scenario $s$ |
| $P_i^{rate}$ | Rate capacity of PV systems of bus $i$ |
| $Pr_{fl,ij}(w(t))$ | Failure probability of the overhead line $ij$ with wind speed $w$ at time $t$ |
| $Pr_{fp,ij,p}(w(t))$ | Failure probability of the pole $p$ at line $ij$ with wind speed $w$ at time $t$ |
| $Pr_{fc,c}(w(t))$ | Failure probability of conductor $c$ between two poles with wind speed $w$ at time $t$ |
| $Pr_{fw,c}(w(t))$ | Direct wind-induced failure probability of conductor $c$ with wind speed $w$ at time $t$ |
| $Pr_{ftr,c}(w(t))$ | Fallen tree-induced failure probability of conductor $c$ with wind speed $w$ at time $t$ |
| $Pr_{u,c}$ | Probability that conductor $c$ is underground |
| $Pr(s)$ | Probability of occurrence for scenario $s$ |
| $p_{ij,\phi}$ | Phases $\phi$ of line between bus $i$ and bus $j$ |
| $Q_i^{ESS,max}$ | Maximum limit of reactive power output of ESS |
| $w(t)$ | Wind speed at time $t$ |
| $m_R$ | Median capacity of conductor |
| $N^{MEG}$ | Number of available MEGs |
| $N^{MES}$ | Number of available MESs |
| $N_i^{MU}$ | Number of mobile units |
| $N_i^{Fuel}$ | Amount of available fuel |
| $N^{Crew}$ | Total number of crews. |
| $N_r^{Crew,max}, N_r^{Crew,min}$ | Maximum and minimum number of available repair crews of region $r$ |
| $N^{conductor}$ | Number of conductor wires between two adjacent poles |
| $N^{pole}$ | Number of distribution poles supporting line |
| $\hat{R}_{ij}, \hat{X}_{ij}$ | Unbalanced three-phase resistance matrix and reactance matrix of line $ij$ |
| $r^F$ | Rate between fuel consumption and power output of generators (L/kWh) |
| $S_i^{PV}$ | PV capacity of bus $i$ |
| $I_r$ | Solar irradiance |
| $U_i^{min}, U_i^{max}$ | Maximum and minimum limits of squared voltage of bus $i$ |
| $\alpha$ | Average tree-induced damage probability of overhead conductor |
| $\xi_R$ | Logarithmic standard deviation of intensity measurement |
| $\eta_{Ch}, \eta_{Dis}$ | ESS charging and discharging efficiencies |

which helps utility companies to prepare resources in advance and mitigate the upcoming extreme weather events. The pre-event preparation can not only avoid high investment cost in long-term planning, but also efficiently reduce the outage duration in post-even restoration.

There are existing studies that have investigated pre-event preparation and resource allocation problems for the resilience enhancement of electric distribution systems. In [24–26], pre-event resource management in MGs and pre-event operation strategies in distribution systems

considered to restore the critical loads and services during power outages in [21–23]. In this paper, we focus on the pre-event preparation,

| $\tau$ | Iteration number of PH |
| $\rho$ | Penalty factor of PH |
| $\epsilon$ | Termination threshold of PH |

**Continuous Variables**

| $E_{i,t,s}^{SOC}$ | SOC of ESS of bus $i$, time $t$ and scenario $s$ |
| $F_{i,s}$ | Total fuel consumption of generators |
| $P_{ij,\phi,t,s}^{K}, Q_{ij,\phi,t,s}^{K}$ | Active/reactive power flows of line $ij$, phase $\phi$, time $t$ and scenario $s$ |
| $P_{i,\phi,t,s}^{G}, Q_{i,\phi,t,s}^{G}$ | Active/reactive power outputs of fuel-based generator of bus $i$, phase $\phi$, time $t$ and scenario $s$ |
| $P_{i,\phi,t,s}^{Ch}, P_{i,\phi,t,s}^{Dis}$ | Active charging/discharging power output of ESS of bus $i$, phase $\phi$, time $t$ of scenario $s$ |
| $Q_{i,\phi,t,s}^{ESS}$ | Reactive power output of ESS of bus $i$, phase $\phi$, time $t$ and scenario $s$ |
| $Q_{i,\phi,t,s}^{PV}$ | Reactive power output of PV of bus $i$, phase $\phi$, time $t$ and scenario $s$ |
| $n_i^{Fuel}$ | Amount of fuel allocated to the generator of bus $i$ |
| $n_r^{Crew}$ | Number of repair crews of region $r$ |
| $U_{i,\phi,t,s}$ | Square of voltage magnitude of bus $i$, phase $\phi$, time $t$ and scenario $s$ |
| $v^{S}$ | Virtual source |
| $v_k^{f}$ | Virtual flow of line $k$ |
| $x, y_s$ | Compact first stage and second stage variables |
| $\bar{x}$ | Expected value of first stage variable |

**Discrete Variables**

| $h_{i,t,s}$ | Binary variable indicating if ESS is charging/discharging (1) or not (0) of bus $i$, phase $\phi$, time $t$ and scenario $s$ |
| $n_i^{MEG}, n_i^{MES}$ | Binary variable indicating if an MEG or MES is allocated (1) or not allocated (0) to bus $i$ |
| $u_{k,t,s}$ | Binary variable indicating if line $k$ is energized (1) or not (0) of time $t$ and scenario $s$ |
| $y_{i,t,s}$ | Binary variable indicating if load is restored (1) or not (0) of bus $i$, phase $\phi$, time $t$ and scenario $s$ |
| $z_{k,t,s}$ | Binary variable indicating if line $k$ is being repaired (1) or not (0) of time $t$ and scenario $s$ |
| $\gamma_{ij,t,s}$ | Binary variable indicating if switch is closed (1) or not (2) of line $ij$, phase $\phi$, time $t$ and scenario $s$ |
| $\chi_{i,t,s}$ | Binary variable indicating if bus $i$ is energized (1) or not (0) of time $t$ and scenario $s$ |

operation actions. The study optimized the topology of the network and the position of crews for upcoming disturbances. In [30] and [31], a two-stage framework is developed to position mobile emergency generators (MEGs) for pre- and post-disasters. Mobile energy storage devices (MESs) are investigated in [32] and [33] for the resilience enhancement of power distribution systems. However, there are limitations in the above studies on pre-event preparation and resource allocation. These limitations are described in the following:

(1) *Pre-event allocation of various flexible resources:* In practice, pre-event preparation includes allocating various flexible resources, such as MEGs, MESs, fuel resources for diesel generators, and repair crews. The optimal allocation of those flexible resources can help utilities to achieve faster and more efficient post-event power restoration. However, previous studies mainly focused on allocating specific flexible resources, rather than formulating a complete optimization problem to pre-allocate various flexible resources together.

(2) *Impacts of solar PV power on system resilience:* Due to intermittent characteristic of traditional distributed energy resources (DERs), such as solar power, PV systems are not considered as a reliable resilient solution [34]. However, the distributed nature of PV power can contribute to a more resilient power system [35]. In practice, PV systems can be coupled with energy storage technologies to enable grid-supporting capability [36], continuous operation during outages [37, 38], and economic operation [39,40]. Different types of PV systems and the impacts of different PV penetration levels on system resilience are ignored in most existing research works.

(3) *Scalability of the solution algorithm:* On one side, the stochastic pre-event preparation model may suffer from computational inefficiency due to a large number of scenarios; on the other side, a limited number of scenarios may influence the stability and quality of the solutions. Therefore, the trade-off between computation time and solution accuracy needs to be studied for stochastic pre-event preparation methods. In addition, a large-scale system is needed to verify the scalability of solution algorithms.

To address these challenges, a two-stage stochastic mixed-integer linear program (SMILP) is proposed for pre-event preparation with the pre-allocation of mobile resources, fuel resources and labor resources. Furthermore, the proposed pre-event preparation model considers different types of PV systems and facilitates the benefits of leveraging high PV penetration for improving the resilience of distribution grids. In this paper, resilience improvement is quantified by the increased served load and reduced outage duration. To deal with the massive computation burden, the proposed two-stage stochastic pre-event preparation problem is solved by a scenario decomposition method, Progressive Hedging (PH) [41], while maintaining the accuracy and stability of the solution [42]. Also, the quality of the solution is validated by the multiple replication procedure (MRP) [43]. The main contribution of this paper is three-folded:

- A two-stage SMILP model is proposed for pre-event preparation for upcoming extreme weather events, where the first stage allocates MEGs, MESs, fuel, and repair crews. The second stage considers distribution system operation and repair crew scheduling constraints.
- The proposed pre-event preparation model considers three types of PV systems during a power outage, including grid-following PV system, hybrid on-grid/off-grid PV system and grid-forming PV system. The improvements of resilience and the reduction of outage duration with different PV penetration levels are also presented.
- The proposed solution algorithm is tested through a solution validation method to show its quality. In addition, a large-scale system, consisting of more than 10,000 nodes, is used to verify the scalability of the proposed pre-event preparation model.

are considered to enhance system resilience during extreme events. In [27], the position and number of depots are determined, and the available resources are managed at the pre-event stage. In [20], repair crews are pre-allocated to depots and integrated with the restoration process for enhancing the response after a disaster. A two-stage stochastic model is developed in [28] to determine staging locations and allocate repair crews for disaster preparation while considering distribution system operation and crew routing constraints. In [29], the authors developed a stochastic model for optimizing pre-event

The remainder of the paper is organized as follows: Section 2 describes the proposed two-stage SMILP for pre-event preparation and resource allocation. Section 3 presents the PH solution algorithm, convergence analysis and solution validation. Case study and results discussion are given in Section 4. Conclusions are provided in Section 5.

## 2. Two-stage stochastic pre-event preparation model

The general framework of the proposed two-stage stochastic pre-event preparation model is shown in Fig. 1. Damage scenarios of extreme weather events are generated based on the following information: (1) identification of extreme weather events, such as flood, hurricane and winter storm; (2) extreme weather event data and metric; (3) fragility model of test systems, which describes the behavior of components under extreme weather events; (4) damage status of components in test systems subject to specific extreme weather events. To approximate the impact of extreme weather events to grid infrastructures, damage scenarios can be generated by mapping the weather data set to the failure probability of grid infrastructures. The Monte Carlo sampling technique can be used to generate a manageable number of scenarios. Adopted from [44], for wind speed $w(t)$, the related failure probability $Pr_{fl,ij}(w(t))$ of overhead line $ij$ can be formulated as follows:

$$Pr_{fl,ij}(w(t)) = 1 - \prod_{p=1}^{N^{pole}} \left(1 - Pr_{fp,ij,p}(w(t))\right) \prod_{c=1}^{N^{conductor}} \left(1 - Pr_{fc,c}(w(t))\right) \quad (1)$$

where $Pr_{fp,ij,p}(w(t))$ and $Pr_{fc,c}(w(t))$ are the failure probability of pole $p$ at line $ij$ and the failure probability of conductor $c$ between two poles, respectively. $N^{pole}$ represents the number of distribution poles supporting line $ij$ and $N^{conductor}$ represents the number of conductor wires between two adjacent poles at line $ij$, respectively. In Eqs. (2) and (3), $Pr_{fp,ij,p}(w(t))$ and $Pr_{fc,c}(w(t))$ can be expressed as follows:

$$Pr_{fp,ij,p}(w(t)) = \Phi\left[\ln(\frac{w(t)/m_R}{\xi_R})\right] \quad (2)$$

$$Pr_{fc,c}(w(t)) = (1 - Pr_{u,c})\max\left(Pr_{fw,c}(w(t)), \alpha Pr_{ftr,c}(w(t))\right) \quad (3)$$

where $\Phi$ is the operator of the log-normal cumulative distribution function (CDF). $m_R$ and $\xi_R$ are the median capacity and the logarithmic standard deviation of intensity measurement, respectively; $Pr_{fw,c}(w(t))$ represents the direct wind-induced failure probability of conductor $c$ and $Pr_{ftr,c}(w(t))$ represents the fallen tree-induced failure probability of conductor $c$. $Pr_{u,c}$ is the probability that conductor $c$ is underground, which is more invulnerable to extreme weather events. $\alpha$ represents the mean probability of tree-induced damage for overhead conductors. More details of weather forecasting methodologies, line fragility models and scenario generation can be found in [45].

As shown in Fig. 1, the proposed SMILP pre-event preparation model has two stages: (i) Flexible resources are pre-allocated for upcoming extreme weather events in the first stage, including the optimal decisions of pre-position and number of MEGs, MESs and repair crews to depots, and allocation of available fuel to generators. (ii) The second stage determines the optimal hourly operation of the distribution systems and assigns repair crews to the damaged components after the extreme weather events. Constraints in the second stage include unbalanced optimal power flow constraints, network reconfiguration and isolation constraints, and repair crew scheduling constraints.

### 2.1. Objective function

The objective function (4) is set to minimize operating cost and maximize the served loads. There are three unit cost coefficients in the objective, unit cost of fuel consumption $C^F$ (L/kWh), unit cost of switching operation $C^{SW}$ ($), and unit cost of load shedding $C_i^D$ at bus $i$ ($/kWh). The objective is formulated as follows:

$$\min \sum_{\forall s} Pr(s)\Big(C^F r^F \sum_{\forall t} \sum_{\forall \phi} \sum_{\forall i} P_{i,\phi,t,s}^G + C^{SW} \sum_{\forall t} \sum_{\forall k \in \Omega_{SW}} \gamma_{ij,t,s}$$
$$+ \sum_{\forall t} \sum_{\forall \phi} \sum_{\forall i} C_i^D (1 - y_{i,t,s}) d_{i,\phi,t}^p\Big) \quad (4)$$

where $Pr(s)$ is the probability of occurrence for scenario $s$. Based on the total number of scenarios $N_s$, $Pr(s)$ can be calculated as $1/|N_s|$. $r^F$ is the rate between fuel consumption and energy output of generators. The unit of $r^F$ is $L/kWh$, which represents the fuel consumption in $L$ per energy generation in $kWh$. $P_{i,\phi,t,s}^G$ is the active power output for fuel-based generator at bus $i$, phase $\phi$, time $t$, and scenario $s$. Binary variable $\gamma_{ij,t,s}$ represents the status of each switch, if a switch on line $ij$ is operated at time $t$, and scenario $s$, then $\gamma_{ij,t,s} = 1$. The binary variable $y_{i,t,s}$ represents the status of load at bus $i$, time $t$, and scenario $s$. If the demand $d_{i,\phi,t}^p$ is served, then $y_{i,t,s} = 1$.

### 2.2. First stage constraints

The first stage constraints revolve around pre-allocating four important resources that will be utilized after an extreme event: (i) MEGs, (ii) MESs, (iii) fuel and (iv) repair crews.

#### 2.2.1. Mobile resources allocation constraints

Mobile resources can be used to restore energy for isolated areas that are not damaged, and to restore critical loads. In addition, fuel management is important after an extreme event to operate emergency generators. Distributing fuel after an extreme event may be difficult due to road conditions. As for repair crews, pre-assigning them to different locations provides a faster and more organized response. The constraints for allocating the mobile resources are modeled as follows:

$$\sum_{\forall i \in \Omega_{CN}} n_i^{MEG} = N^{MEG} \quad (5)$$

$$\sum_{\forall i \in \Omega_{CN}} n_i^{MES} = N^{MES} \quad (6)$$

$$n_i^{MEG} + n_i^{MES} \le N_i^{MU}, \forall i \in \Omega_{CN} \quad (7)$$

where binary variables $n_i^{MEG}$ and $n_i^{MES}$ equal 1 if a MEG or MES are allocated to bus $i$, respectively. The set $\Omega_{CN}$ represents the set of candidate buses for MEGs and MESs. Constraints (5) and (6) indicates that the number of installed MEGs and MESs are equal to the number of available devices ($N^{MEG}$ and $N^{MES}$). In this work, it assumes that each bus can only have a limited number of mobile units $N_i^{MU}$, which is enforced by (7).

#### 2.2.2. Fuel resources allocation constraints

Define the set $\Omega_G = \Omega_{EG} \cup \Omega_{CN}$, where $\Omega_{EG}$ is the set of buses that have fuel-based emergency generators. The fuel allocated to $\Omega_G$ must be limited to the available amount of fuel. The fuel allocation constraints are presented as follows:

$$\sum_{\forall i \in \Omega_G} n_i^{Fuel} \le N^{Fuel} \quad (8)$$

$$F_i^G \le n_i^{Fuel} \le F_i^{max}, \forall i \in \Omega_G \quad (9)$$

Constraint (8) limits the total amount of allocated fuel to the available amount of fuel ($N^{Fuel}$), where $n_i^{Fuel}$ is the amount of fuel allocated to the generator at bus $i$. In this work, it assumes that not all the available fuel needs to be allocated. Constraint (9) limits the amount of fuel on each site, where $F_i^G$ is the amount of fuel already present for the generator at bus $i$, and $F_i^{max}$ represents the maximum capacity of
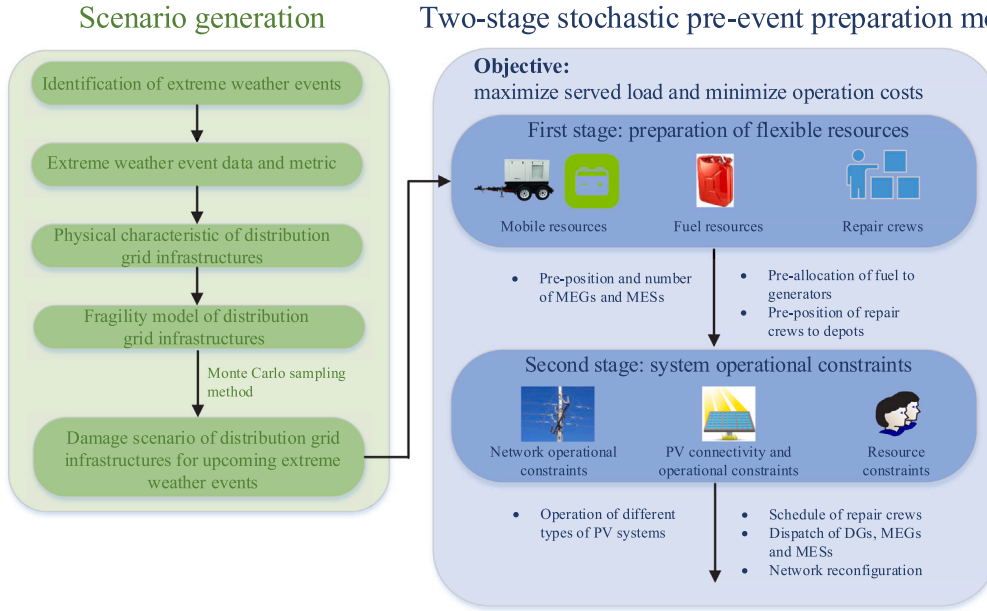
**Fig. 1.** The proposed two-stage stochastic pre-event preparation model.

fuel at bus *i*. Note that the aim of fuel allocation is to decide how much fuel should be allocated to the generators, which have defined locations in the system. Therefore, the logistic process of transferring the fuel to the generators is not considered in this paper, as this problem can be solved as a separate problem.

### 2.2.3. Repair crew allocation constraints

To allocate the repair crews, our model divides the network into different regions $\Omega_R$. Each region will be assigned with different crews, who will conduct the repairs in that region. Note that the buses in a single region should be relatively close to each other. These regions should be determined based on the physical distances between the buses. Then the crews are allocated to the regions, where the crews would be stationed at a depot. Therefore, the distance is not explicitly considered in the mathematical model, but it is considered in the preprocessing step of determining the regions.

Constraint (10) states that the total crews deployed to all regions is equal to the number of available crews. This constraint can be relaxed by replacing the equality with an inequality if some crews are required on standby. This work assumes that all available crews will be deployed. Constraint (11) sets a minimum and maximum number of crews that can be stationed in each individual region.

$$\sum_{\forall r \in \Omega_R} n_r^{\text{Crew}} = N^{\text{Crew}} \tag{10}$$

$$N_r^{\text{Crew,min}} \le n_r^{\text{Crew}} \le N_r^{\text{Crew,max}}, \forall r \in \Omega_R \tag{11}$$

where $n_r^{\text{Crew}}$ is the number of repair crews in region *r* and $N^{\text{Crew}}$ is the total number of crews. The number of repair crews is limited in each region, using $N_r^{\text{Crew,min}}$ and $N_r^{\text{Crew,max}}$, depending on the size and capacity of the staging locations.

After allocating the fuel in the first stage, each generator can be operated in the second stage based on how much fuel is available. Similarly, once the pre-position decisions of mobile resources and repair crews are obtained in the first stage, the second stage can decide the mobile resource operation and repair schedule.

### 2.3. Second stage constraints

In the second stage of the proposed pre-event preparation model, the constraints of PV systems and repair crew dispatch are mainly discussed. The model also considers unbalanced power flow constraints, voltage constraints, and network reconfiguration constraints [43,46].

### 2.3.1. PV system constraints

To thoroughly investigate the impact of PV systems on system resilience, three types of PV systems are considered with different operation modes in the second stage [43], $\Omega_{\text{PV}} = \Omega_{\text{PV}}^G \cup \Omega_{\text{PV}}^H \cup \Omega_{\text{PV}}^C$. The main differences between those three types of PV systems are their different behaviors during an outage: (i) Type 1: on-grid PV with grid-following operation mode ($\Omega_{\text{PV}}^G$), where the PV will be switched off and disconnected during an outage. (ii) Type 2: hybrid on-grid/off-grid PV + energy storage system (ESS) ($\Omega_{\text{PV}}^H$), where the PV system operates on-grid in normal condition or off-grid during an outage (serves local load only). (iii) Type 3: grid-forming PV + ESS with grid-forming capability ($\Omega_{\text{PV}}^C$), this system can restore part of the network that is not damaged if the fault is isolated. There are several benefits of considering different types of PV systems during a power outage. For example, this kind of model is more like a real-world application with multiple PV systems. In addition, the PV systems are mostly considered as power supply resources in previous research works, while the grid-forming and black-start capability of PV systems during outages shall also be explored and discussed. The output power of the PV systems is determined using the following equations:

$$0 \le P_{i,\phi,t,s}^{\text{PV}} \le \frac{I_{r_{i,t,s}}}{1000 \text{ W/m}^2} P_i^{\text{rate}}, \forall i \in \Omega_{\text{PV}}/\Omega_{\text{PV}}^G, \phi, t, s \tag{12}$$

$$0 \le P_{i,\phi,t,s}^{\text{PV}} \le \chi_{i,t,s} \frac{I_{r_{i,t,s}}}{1000 \text{ W/m}^2} P_i^{\text{rate}}, \forall i \in \Omega_{\text{PV}}^G, \phi, t, s \tag{13}$$

$$(P_{i,\phi,t,s}^{\text{PV}})^2 + (Q_{i,\phi,t,s}^{\text{PV}})^2 \le (S_i^{\text{PV}})^2, \forall i \in \Omega_{\text{PV}}/\Omega_{\text{PV}}^G, \phi, t, s \tag{14}$$

$$(P_{i,\phi,t,s}^{\text{PV}})^2 + (Q_{i,\phi,t,s}^{\text{PV}})^2 \le \chi_{i,t,s}(S_i^{\text{PV}})^2, \forall i \in \Omega_{\text{PV}}^G, \phi, t, s \tag{15}$$

The PV active power output $P_{i,\phi,t,s}^{\text{PV}}$ depends on the solar cell rating capacity $P^{\text{rate}}$ and the solar irradiance $I_{r_{i,t,s}}$ [47]. The active power outputs of Type 2 $\Omega_{\text{PV}}^H$ and Type 3 $\Omega_{\text{PV}}^C$ PVs can be determined in (12), while the active power outputs of Type 1 $\Omega_{\text{PV}}^G$ PVs is calculated in (13). The binary variable $\chi_{i,t,s} = 0$ if bus *i* is not energized at time

$t$ and scenario $s$. Using advanced PV smart inverters [48], the PVs can provide reactive power support $Q_{i,\phi,t,s}^{\mathrm{PV}}$, which is constrained by the capacity $S_i^{\mathrm{PV}}$ in (14) and (15). During an outage, on-grid PVs are disconnected and the on-site load is not served by the PVs, therefore, constraints (13) and (15) are multiplied by $\chi_{i,t,s}$. PV systems of types $\Omega_{\mathrm{PV}}^{\mathrm{C}}$ and $\Omega_{\mathrm{PV}}^{\mathrm{H}}$ can disconnect from the grid and serve the on-site load.

An example network with a damaged line is given in Fig. 2, where the network is divided into three islands due to the damaged line. The grid-forming sources in $\Omega_{\mathrm{PV}}^{\mathrm{C}} \cup \Omega_{\mathrm{G}}$ has the black start capability and can restore the network. While PV system in types $\Omega_{\mathrm{PV}}^{\mathrm{G}}$ or $\Omega_{\mathrm{PV}}^{\mathrm{H}}$ can connect to the grid only after the PV bus is energized. Island A has a grid-forming generator, therefore, a microgrid is created and the PV system can participate. Island B must be isolated because of the damaged line. Island C does not have any grid-forming generators; hence, it will not be active and the grid-tied PV will be disconnected.

To determine the connection status of the PV systems, a virtual network is designed in parallel to the distribution network. The example network shown in Fig. 2 is transformed into a virtual network shown in Fig. 3. To identify if an island network can be energized and restored by grid-forming sources $\Omega_{\mathrm{PV}}^{\mathrm{C}} \cup \Omega_{\mathrm{G}}$, a virtual network is built with virtual sources, virtual flows, and virtual loads. Each grid-forming generator is replaced by a virtual source with infinite capacity. Other power sources without grid-forming capability (e.g., grid-tied PVs) are removed. The virtual loads with magnitude of 1 replace the actual loads. The virtual network scheme is modeled using constraints (16)–(20).

$$\sum_{\forall j \in \Omega_{\mathrm{PV}}^{\mathrm{C}} \cup \Omega_{\mathrm{G}}} v_{j,t,s}^{\mathrm{S}} + \sum_{\forall k \in \Omega_{\mathrm{K}}(.,i)} v_{k,t,s}^{\mathrm{f}} = \chi_{i,t,s} + \sum_{\forall k \in \Omega_{\mathrm{K}}(i,.)} v_{k,t,s}^{\mathrm{f}}, \forall i,t,s \tag{16}$$

$$-(u_{k,t,s})M \le v_{k,t,s}^{\mathrm{f}} \le (u_{k,t,s})M, \forall k \in \Omega_{\mathrm{K}}, t, s \tag{17}$$

$$0 \le v_{k,t,s}^{\mathrm{S}} \le (n_i^{\mathrm{MEG}} + n_i^{\mathrm{MES}})M, \forall i \in \Omega_{\mathrm{CN}}, t, s \tag{18}$$

$$\chi_{i,t,s} \ge y_{i,t,s}, \forall i \in \Omega_{\mathrm{N}}/\{\Omega_{\mathrm{PV}}^{\mathrm{C}} \cup \Omega_{\mathrm{PV}}^{\mathrm{H}} \cup \Omega_{\mathrm{G}}\}, t, s \tag{19}$$

$$\chi_{i,t,s} + n_i^{\mathrm{MEG}} + n_i^{\mathrm{MES}} \ge y_{i,t,s}, \forall i \in \Omega_{\mathrm{CN}}, t, s \tag{20}$$

A power balance equation is added for each virtual bus, which means that if the virtual load at a bus is served, then that bus is energized. Therefore, for islands without grid-forming generators, all buses will be de-energized as the virtual loads in the island cannot be served. Constraint (16) is the node balance constraint for the virtual network. Virtual source $v^{\mathrm{S}}$ is connected to buses with power sources that have the capability to restore the system. The variable $v_k^{\mathrm{f}}$ represents the virtual flow on line $k$ and each bus is given a load of 1 that is multiplied by $\chi_i$. Therefore, $\chi_i = 1$ (bus $i$ is energized) if the virtual load can be served by a virtual source and 0 (bus $i$ is de-energized) otherwise. The virtual flow is limited by (17). The limits are multiplied by the status of the line $(u_{k,t,s})$ so that the virtual flow is 0 if a line is disconnected. The virtual source can be used only if a generator is installed, as enforced by (18). Define $\Omega_{\mathrm{N}}$ as the set of all buses. If bus $i$ is de-energized, then the load must be shed (19), unless bus $i$ has a local power source with disconnect switch. Constraint (20) is similar to (19) but with the presence of mobile sources.

### 2.3.2. Repair crews constraints

The second stage of the proposed pre-event model assigns repair crews to damaged components that are in the area at where the crews are positioned. Note that the travel time is neglected in this study, as the travel distances between components in the same area is assumed to be small. An example for crew assignment is given in Fig. 4, where two working areas are assigned for the crews. In this example, four damaged lines in Area 1 will be repaired by crews 1–3, while crews 4

and 5 are responsible for the two damaged lines in Area 2. The repair crews constraints can be presented as follows:

$$\sum_{\forall k \in \Omega_{\mathrm{DL}(s)}} z_{k,t,s} \le n_r^{\mathrm{Crew}}, \forall r, t, s \tag{21}$$

$$\sum_{\forall t} z_{k,t,s} \le T_{k,s}^r, \forall k \in \Omega_{\mathrm{DL}(s)}, s \tag{22}$$

$$\frac{1}{T_{k,s}^r} \sum_{\tau=1}^{t-1} z_{k,\tau,s} - 1 + \epsilon \le u_{k,t,s} \le \frac{1}{T_{k,s}^r} \sum_{\tau=1}^{t-1} z_{k,\tau,s}, \forall k \in \Omega_{\mathrm{DL}(s)}, t, s \tag{23}$$

where $z_{k,t,s}$ is a binary variable, $z_{k,t,s} = 1$ means that line $k$ is being repaired at time $t$ on scenario $s$, and $\Omega_{\mathrm{DL}(s)}$ is the set of damaged lines on scenario $s$. Constraint (21) limits the number of repairs being conducted in each area according to the number of crews $n_r^{\mathrm{Crew}}$ available. Constraint (22) defines the repair time for each damaged line. The line status $u_{k,t,s}$ equals 0 until the repair process is conducted for $T_{k,s}^r$ time periods. Based on constraint (23), let $T_{k,s}^r = 3$, $z_{k,t,s} = \{0,0,1,1,1,0,0\}$, then $u_{k,t,s} = \{0,0,0,0,0,1,1\}$. For example, when $t = 6$ and $\epsilon = 0.001$, then constraint (23) becomes $0.668 \le u_{k,6,s} \le 1$, therefore, $u_{k,6,s} = 1$.

### 2.3.3. Network operational constraints

The next set of constraints are related to the operation of distribution systems, including unbalanced power flow equations, radiality constraints, fuel consumption, and energy storage constraints. The unbalanced distribution system constraints are given below:

$$\sum_{b \in \Omega_{\mathrm{K}}(i,.)} P_{b,\phi,t,s}^{\mathrm{K}} - \sum_{k \in \Omega_{\mathrm{K}}(.,i)} P_{k,\phi,t,s}^{\mathrm{K}} = P_{i,\phi,t,s}^{\mathrm{G}} + P_{i,\phi,t,s}^{\mathrm{PV}}$$
$$+ (P_{i,\phi,t,s}^{\mathrm{Ch}} - P_{i,\phi,t,s}^{\mathrm{Dis}}) - y_{i,t,s} d_{i,\phi,t}^P, \forall i, \phi, t, s \tag{24}$$

$$\sum_{b \in \Omega_{\mathrm{K}}(i,.)} Q_{b,\phi,t,s}^{\mathrm{K}} - \sum_{k \in \Omega_{\mathrm{K}}(.,i)} Q_{k,\phi,t,s}^{\mathrm{K}} = Q_{i,\phi,t,s}^{\mathrm{G}} + Q_{i,\phi,t,s}^{\mathrm{PV}}$$
$$+ Q_{i,\phi,t,s}^{\mathrm{ESS}} - y_{i,t,s} d_{i,\phi,t}^Q, \forall i, \phi, t, s \tag{25}$$

$$-u_{k,t,s} P_k^{\mathrm{K,max}} \le P_{k,\phi,t,s}^{\mathrm{K}} \le u_{k,t,s} P_k^{\mathrm{K,max}}, \forall k \in \Omega_{\mathrm{K}}, \phi, t, s \tag{26}$$

$$-u_{k,t,s} Q_k^{\mathrm{K,max}} \le Q_{k,\phi,t,s}^{\mathrm{K}} \le u_{k,t,s} Q_k^{\mathrm{K,max}}, \forall k \in \Omega_{\mathrm{K}}, \phi, t, s \tag{27}$$

$$0 \le P_{i,\phi,t,s}^{\mathrm{G}} \le P_i^{\mathrm{G,max}}, \forall i \in \Omega_{\mathrm{EG}}, \phi, t, s \tag{28}$$

$$0 \le Q_{i,\phi,t,s}^{\mathrm{G}} \le Q_i^{\mathrm{G,max}}, \forall i \in \Omega_{\mathrm{EG}}, \phi, t, s \tag{29}$$

$$0 \le P_{i,\phi,t,s}^{\mathrm{G}} \le n_i^{\mathrm{MEG}} P_i^{\mathrm{G,max}}, \forall i \in \Omega_{\mathrm{CN}}, \phi, t, s \tag{30}$$

$$0 \le Q_{i,\phi,t,s}^{\mathrm{G}} \le n_i^{\mathrm{MEG}} Q_i^{\mathrm{G,max}}, \forall i \in \Omega_{\mathrm{CN}}, \phi, t, s \tag{31}$$

$$U_{i,\phi,t,s} - U_{j,\phi,t,s} \ge 2(\hat{R}_{ij} P_{ij,\phi,t,s}^{\mathrm{K}} + \hat{X}_{ij} Q_{ij,\phi,t,s}^{\mathrm{K}})$$
$$+ (u_{k,t,s} + p_{ij,\phi} - 2)M, \forall k, ij \in \Omega_{\mathrm{K}}, \phi, t, s \tag{32}$$

$$U_{i,\phi,t,s} - U_{j,\phi,t,s} \le 2(\hat{R}_{ij} P_{ij,\phi,t,s}^{\mathrm{K}} + \hat{X}_{ij} Q_{ij,\phi,t,s}^{\mathrm{K}})$$
$$+ (2 - u_{k,t,s} - p_{ij,\phi})M, \forall k, ij \in \Omega_{\mathrm{K}}, \phi, t, s \tag{33}$$

$$\chi_{i,t,s} U_i^{\min} \le U_{i,\phi,t,s} \le \chi_{i,t,s} U_i^{\max}, \forall i, \phi, t, s \tag{34}$$
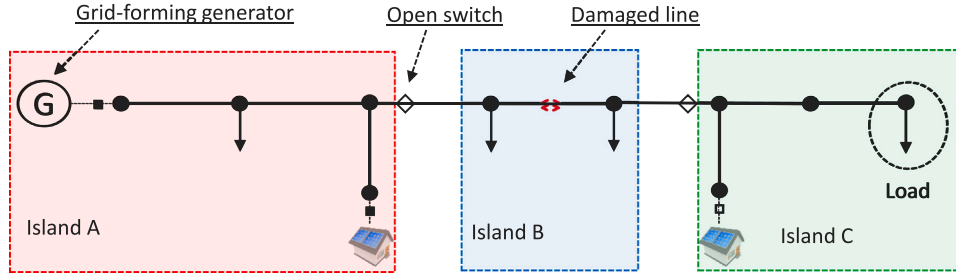
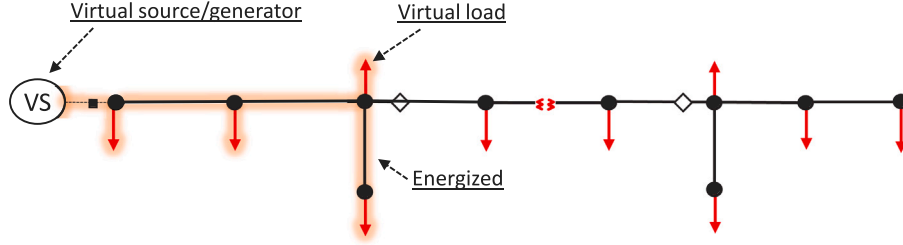**Fig. 2.** A single line diagram of an example network with one damaged line.



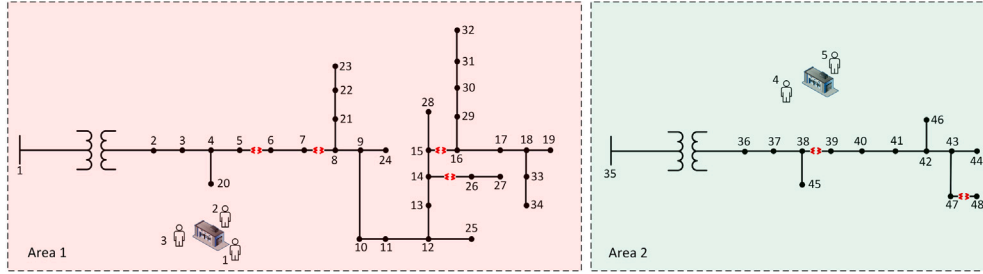**Fig. 3.** A virtual network created for the example network in Fig. 2.



**Fig. 4.** A crew assignment example with 2 depots and 5 crews.

$$\sum_{k \in \Omega_{B(l)}} u_{k,t,s} \leq |\Omega_{B(l)}| - 1, \forall l \in \Omega_{loop}, t, s \tag{35}$$

Constraints (24) and (25) are nodal power balance constraints of active and reactive powers, where $P_{ij,\phi,t,s}^K$ and $Q_{ij,\phi,t,s}^K$ are active and reactive power flows, and $P_{i,\phi,t,s}^G$ and $Q_{i,\phi,t,s}^G$ are the power outputs of the generators. The active charging/discharging and reactive power outputs of energy storage systems are denoted by $P_{i,\phi,t,s}^{Ch}$, $P_{i,\phi,t,s}^{Dis}$ and $Q_{i,\phi,t,s}^{ESS}$. Constraints (26)–(27) represent the active and reactive power limits of the lines, where the limits ($P_k^{K,max}$ and $Q_k^{K,max}$) are multiplied by the line status binary variable $u_{k,t,s}$. Therefore, if a line is disconnected or damaged, power cannot flow through it. Constraints (28)–(29) limit the output of the generators to $P_i^{G,max}$ and $Q_i^{G,max}$. Similarly, the output of the MEGs is limited in (30)–(31) if an MEG is installed ($n_i^{MEG} = 1$).

Constraints (32) and (33) calculate the voltage difference along line $k$ between bus $i$ and bus $j$, where $U_{i,\phi,t,s}$ is the square of voltage magnitude of bus $i$. The big-M method is used to relax constraints (32) and (33), if lines are damaged or disconnected. $\hat{R}_{ij}$ and $\hat{X}_{ij}$ are the unbalanced three-phase resistance matrix and reactance matrix of line $ij$, which can be referred to in [48]. The vector $p_{ij,\phi}$ represents the phases of line $ij$. Constraint (34) guarantees that the voltage is limited within a specified region ($U_i^{min}$ and $U_i^{max}$), and is set to 0 if the bus is in an outage area. Constraint (35) can guarantee the radiality network during the network reconfiguration. This model assumes that all the possible loops can be identified by the depth-first search method. The set of loops are given by $\Omega_{loop}$, and the set of switches in loop $l$ is given by $\Omega_{B(l)}$. For each fuel-based generator, the total fuel consumption $F_{i,s}$

is limited by the available fuel resources $n_i^{Fuel}$ in constraint (36), as follows:

$$F_{i,s} = r^f \sum_{\forall t} \sum_{\forall \phi} P_{i,\phi,t,s}^G \leq n_i^{Fuel}, \forall i \in \Omega_G, \phi, t, s \tag{36}$$

The operation constraints for ESSs and MESs include the change in state of charge (SOC), charging and discharging limits, and reactive power limits. Let $\Omega_{ES}$ be the set of buses with ESSs, and $\Omega_{ESC} = \Omega_{ES} \cup \Omega_{CN}$.

$$E_{i,t,s}^{SOC} = E_{i,t-1,s}^{SOC} + \Delta t \frac{(\sum_{\forall \phi} P_{i,\phi,t,s}^{Ch} \eta_{Ch} - \sum_{\forall \phi} P_{i,\phi,t,s}^{Dis} / \eta_{Dis})}{E_i^{Cap}}, \forall i \in \Omega_{ESC}, \phi, t, s \tag{37}$$

$$E_i^{SOC,min} \leq E_{i,t,s}^{SOC} \leq E_i^{SOC,max}, \forall i \in \Omega_{ESC}, t, s \tag{38}$$

$$0 \leq P_{i,\phi,t,s}^{Ch} \leq h_{i,t,s} P_i^{Ch,max}, \forall i \in \Omega_{ESC}, \phi, t, s \tag{39}$$

$$0 \leq P_{i,\phi,t,s}^{Dis} \leq (1 - h_{i,t,s}) P_i^{Dis,max}, \forall i \in \Omega_{ESC}, \phi, t, s \tag{40}$$

$$-Q_i^{ESS,max} \leq Q_{i,\phi,t,s}^{ESS} \leq Q_i^{ESS,max}, \forall i \in \Omega_{ES}, \phi, t, s \tag{41}$$

$$0 \leq P_{i,\phi,t,s}^{Ch} \leq n_i^{MES} P_i^{Ch,max}, \forall i \in \Omega_{CN}, \phi, t, s \tag{42}$$

$$0 \leq P_{i,\phi,t,s}^{\mathrm{Dis}} \leq n_i^{\mathrm{MES}} P_i^{\mathrm{Dis,max}}, \forall i \in \Omega_{\mathrm{CN}}, \phi, t, s \tag{43}$$

$$-n_i^{\mathrm{MES}} Q_i^{\mathrm{ESS,max}} \leq Q_{i,\phi,t,s}^{\mathrm{ESS}} \leq n_i^{\mathrm{MES}} Q_i^{\mathrm{ESS,max}}, \forall i \in \Omega_{\mathrm{CN}}, \phi, t, s \tag{44}$$

Constraint (37) calculates the state of charge (SOC) of ESSs ($E_{i,t,s}^{\mathrm{SOC}}$). $E_i^{\mathrm{Cap}}$ is the maximum capacity of the storage system. To ensure safe ESS operation, the SOC and charging ($P_{i,\phi,t,s}^{\mathrm{Ch}}$) and discharging ($P_{i,\phi,t,s}^{\mathrm{Dis}}$) power of ESSs are constrained as shown in (38)–(40). Here, $E_i^{\mathrm{SOC,min}}$, $E_i^{\mathrm{SOC,max}}$, $P_i^{\mathrm{Ch,max}}$ and $P_i^{\mathrm{Dis,max}}$ define the permissible range of SOC, and maximum charging and discharging power, respectively. In constraints (39)–(40), the binary variable $h_{i,t,s}$ indicates that ESSs cannot charge and discharge at the same time instant. The ESS charging and discharging efficiency are represented by $\eta_{\mathrm{Ch}}$ and $\eta_{\mathrm{Dis}}$, respectively. The reactive power of ESS, $Q_{i,\phi,t,s}^{\mathrm{ESS}}$, is kept within maximum limit, $Q_i^{\mathrm{ESS,max}}$, through constraint (41). For MES units, the constraints (42)–(43) are presented so that if $n_i^{\mathrm{MES}} = 0$, the output power is 0 at bus $i$. The same method is applied for the reactive power in (44).

## 3. Solution algorithm

When the number of scenarios is finite, a two-stage stochastic problem can be modeled as a single-stage large linear programming model, where each constraint in the problem is duplicated for each realization of the random data. As discussed before, the Monte Carlo sampling technique can be used to generate a manageable number of scenarios for problems where the number of realizations is too large or infinite. In this work, the scenario decomposing method PH is used to solve the proposed two-stage stochastic pre-event preparation problem.

### 3.1. Two-stage progressive hedging algorithm

The proposed two-stage stochastic pre-event preparation model (4)–(44) can be compactly reformulated as follows:

$$\xi = \min_{x,y_s} a^T x + \sum_{\forall s} Pr(s) b_s^T y_s \tag{45}$$

s.t. $(x, y_s) \in Q_s, \forall s$ (46)

In objective (45), the vectors $a$ and $b_s$ include the coefficients related with the compact first stage variable $x$ and compact second stage variable $y_s$, respectively. The compact constraint (46) can ensure the feasibility for solutions from each subproblem and scenario. When the non-anticipativity of the first stage variables is relaxed, then the PH algorithm decomposes the extensive form (EF) (45)–(46) into scenario-based subproblems. Therefore, the proposed stochastic pre-event preparation problem with the total number $S$ of scenarios can be decomposed into $S$ subproblems. In Algorithm 1, the proposed stochastic pre-event preparation problem is solved by PH algorithm. In Step 1, we initialize the problem. In Step 2–3, the subproblems with individual scenarios are solved. In Step 4, we obtain the expected value $\bar{x}$ of the first stage solution by aggregating the solutions from Steps 2–3. Step 5 calculates the value of the multiplier $\eta_s$. In Step 8, the subproblems are solved by augmenting two terms: one linear term, which is proportional to the multiplier $\eta_s^{\tau-1}$; one squared two norm term of the difference between $x$ and $\bar{x}^{\tau-1}$, which is penalized by *rho*. Steps 9–10 are similar as Steps 4–5. The algorithm terminates once all first stage decisions $x_s$ converge to a common $\bar{x}$. Note that the two-stage model has been reformulated to a single-level problem for each individual scenario. In Algorithm 1, $\tau$ is the iteration number, $\rho$ is a penalty factor and $\epsilon$ is the threshold value for termination.

**Algorithm 1** PH Algorithm for Solving Stochastic Pre-event Preparation Problem

1: **Initialization**: the iteration $\tau$.
2: For each individual scenario $s \in S$, solve.
3: $x_s^{(\tau)} := \mathrm{argmin}_x \{a^T x + b_s^T y_s : (x, y_s) \in Q_s\}$.
4: $\bar{x}^{(\tau)} := \sum_{\forall s \in S} Pr(s) x_s^{(\tau)}$.
5: $\eta_s^{(\tau)} := \rho(x_s^{(\tau)} - \bar{x}^{(\tau)})$.
6: $\tau := \tau + 1$.
7: For each individual scenario $s \in S$, solve.
8: $x_s^{(\tau)} := \mathrm{argmin}_x \{a^T x + b_s^T y_s + \eta_s^{(\tau-1)} x + \frac{\rho}{2} \|x_s^{(\tau)} - \bar{x}^{(\tau)}\|^2 : (x, y_s) \in Q_s\}$.
9: $\bar{x}^{(\tau)} := \sum_{\forall s \in S} Pr(S) x_s^{(\tau)}$.
10: $\eta_s^{(\tau)} := \eta_s^{(\tau-1)} + \rho(x_s^{(\tau)} - \bar{x}^{(\tau)})$.
11: **if** $\sum_{\forall s \in S} Pr(s) \|x_s^{(\tau)} - \bar{x}^{(\tau)}\| \leq \epsilon$ **then**
12: Go to Step 5.
13: **else**
14: terminate.
15: **end if**

**Algorithm 2** Multiple Replication Procedure

1: **Initialization**: Set $\alpha \in (0, 1)$ (e.g., $\alpha = 0.05$), sample size $n$, replication size $n_g$ and a candidate solution $\hat{x} \in X$.
2: For $k = 1, 2, ..., n_g$.
3: Sample i.i.d. observations $\zeta^{k_1}, \zeta^{k_2}, ..., \zeta^{k_n}$ from the distribution of $\zeta$.
4: Solve ($\mathrm{SP_n}$) using $\zeta^{k_1}, \zeta^{k_2}, ..., \zeta^{k_n}$ to obtain $x_n^{k*}$.
5: Calculate $G_n^k(\hat{x}) := n^{-1} \sum_{j=1}^n (f(\hat{x}, \zeta^{kj}) - f(x_n^{k*}, \zeta^{kj}))$.
6: End for.
7: Calculate gap estimate $\bar{G}_n(n_g) := \frac{1}{n_g} \sum_{k=1}^{n_g} G_n^k(\hat{x})$.
8: Calculate sample variance $s_G^2(n_g) := \frac{1}{n_g-1} \sum_{k=1}^{n_g} (G_n^k(\hat{x}) - \bar{G}_n(n_g))^2$.
9: Let $\epsilon := t_{n_g-1,\alpha} S_G(n_g)/\sqrt{n_g}$.
10: Obtain one-sided CI on $[0, \bar{G}_n(n_g) + \epsilon_g]$.
11: **Output**: Approximate $(1 - \alpha)$ as the level confidence interval on $\mu_{\hat{x}}$.

### 3.2. Convergence analysis and solution validation

As shown in Algorithm 1, the convergence metric $g^\tau$ for the progressive hedging algorithm at each iteration $\tau$ is expressed as the deviation from the mean summed across all first stage variables $x_s(\tau)$ and the average value of the first stage variable $\bar{x}^\tau$ as follows:

$$g^\tau = \sum_{s \in S} Pr(s) \|x_s(\tau) - \bar{x}^\tau\| \tag{47}$$

Since the solution is obtained using a limited number of damage scenarios, the quality of the solution requires verification. Adopted from [49], the MRP can be applied to repeat generating $S$ scenarios and solving the proposed model for $S$ times. Then the confidence interval (CI) is constructed to calculate the optimality gap. The detailed steps in MRP are shown in Algorithm 2, where $\bar{G}_n(n_g)$ is the gap estimate and $s_G^2(n_g)$ is the sample variance. Numerical results for the convergence analysis and solution validation of the test case are given in the next section.

## 4. Case study

This section uses a large-scale system as a test case to verify the scalability and effectiveness of the two-stage stochastic pre-event preparation model. This large-scale system consists of 3 existing test systems, EPRI ckt5, ckt7 systems [50], and IEEE 8500 bus system [51], Following the suggestions from [15], the unit costs in the simulation are $C^{\mathrm{D}} = 14\$/$kWh for load shedding at all buses, $C^{\mathrm{SW}} = 8\$$ for each line switch, $C^{\mathrm{F}} = 1\$/$L and $r^{\mathrm{F}} = 0.3$ L/kWh for fuel consumption of generators. The Pyomo and Gurobi mixed-integer solver [52] are used to solve the proposed stochastic model. All experiments are implemented on the
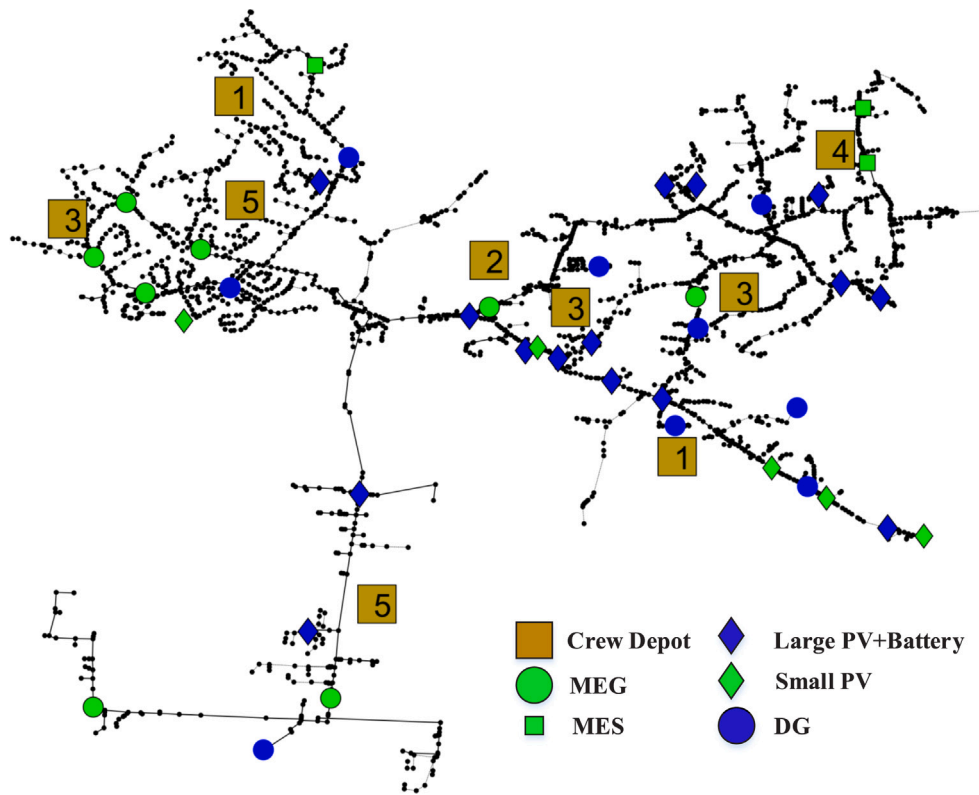
**Fig. 5.** Resource allocation of large-system with the proposed model.
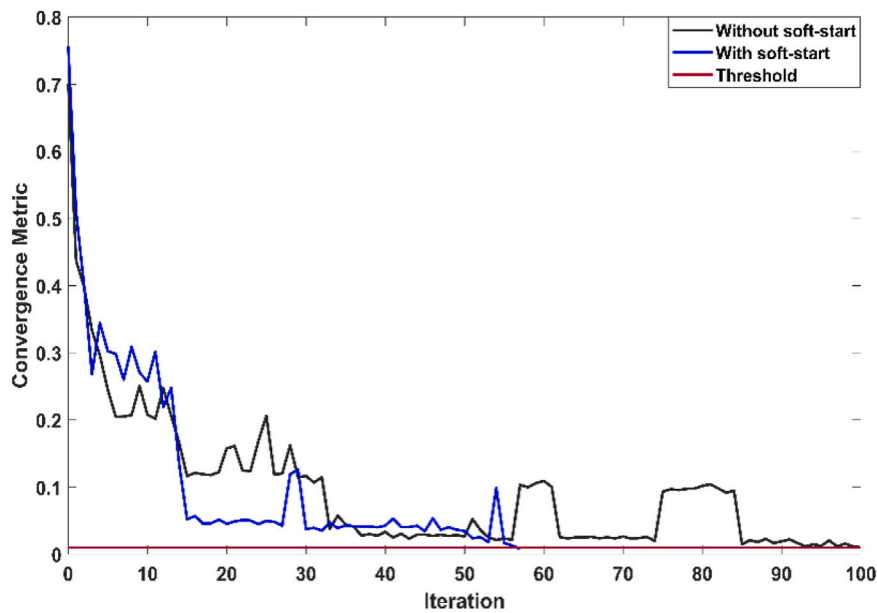


**Fig. 6.** The convergence metric comparison with and without soft-start solutions.

Iowa State University Condo cluster, whose individual blade consists of two 2.6 GHz 8-Core Intel E5-2640 v3 processors and 128 GB of RAM.

### 4.1. Pre-event preparation results

This case study include 9 depots that are hosting a total of 27 crews, 9 dispatchable DGs, 8 MEGs, 3 MESs, 123 switches, 5 small PVs, 15 large PVs, and 12 ESSs. The active and reactive power capacities of the 9 DGs are 300 kW and 250 kVAr. The active power capacity of small PVs ranges from 11 kW to 22 kW. The active power capacity of large

PVs is 500 kW. The 12 ESSs are rated at 500 kW/ 3500 kWh. The pre-event preparation model of the large-scale system is solved in 10.2 h with 10 damage scenarios. The locations of MEGs, MESs, and number of crews are shown in Fig. 5. 27 crews are allocated to 9 different depots. The value inside the crew depot in Fig. 5 represents the number of crews assigned to that depot. Areas with a large number of crews indicate that the lines in the area have high damage probabilities.

As discussed in Section 3.2, the convergence metric can be used to evaluate the convergence speed of the proposed model. At the same time, the computational speed with and without a soft-start solution are
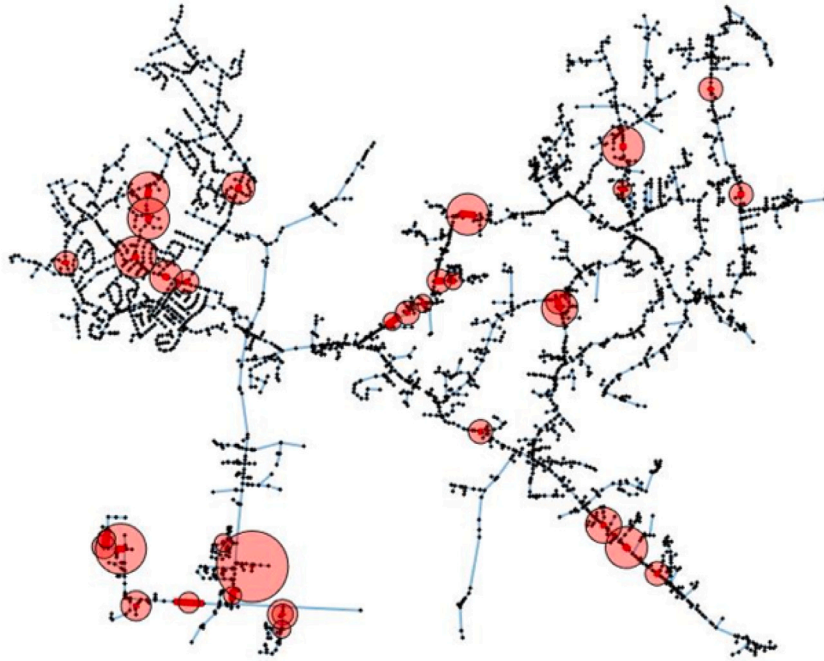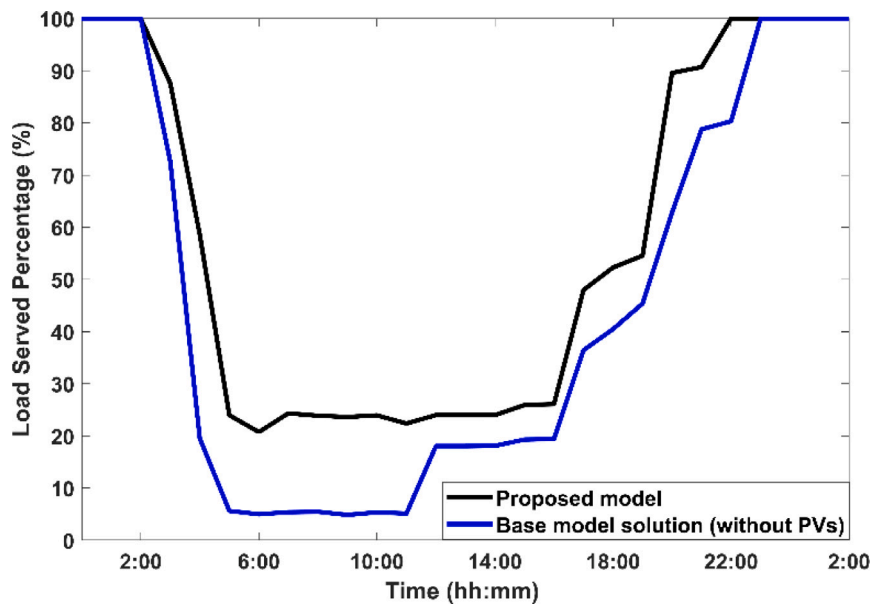
**Fig. 7.** Aggregated damaged areas.



**Fig. 8.** Comparison between the base model and the proposed method.

compared. In this paper, a soft-start solution means that the previously computed solution in other instances will be used as the starting point. The comparison result is shown in Fig. 6. If the convergence metric reaches the convergence threshold of 0.01, the algorithm will stop and obtain the optimal solution. The instance with a soft-start solution converges at 57 iterations and takes 10.2 h. The case without a soft-start solution converges after 100 iterations and takes 24.3 h. To test the solution quality with MRP, based on the limited number of generated damage scenarios, the one-sided CI of the obtained solution is $[0, 12.48\%]$. This small gap indicates that the damage scenarios are representative and the solution is stable with high quality.

To evaluate the performance of the developed pre-event preparation model, the model is compared to a base model. The base case is generated by the following steps: (i) one MEG is pre-positioned at each substation. (ii) Extra MEGs are pre-positioned at high-priority loads. (iii) PV and ESS are not considered. (iv) Fuel is allocated to the MEGs such that the MEGs can operate for at least 24 h. (v) Crews are allocated evenly between depots. In this work, the average outage duration is calculated by dividing the sum of outage duration for the loads by the total number of loads. To compare the proposed model and the base model, a random scenario is generated and test the response of the system. The generated scenario has 103 damaged lines, which are aggregated to 34 damaged areas in Fig. 7. Each circle represents the repair time needed for the specific damaged area considering all the aggregated damaged lines.

The comparison between the base model and the proposed method is shown in Fig. 8. In the base model, the total restored energy is 231,422.38 kWh and the average outage duration is 14.69 h. In the
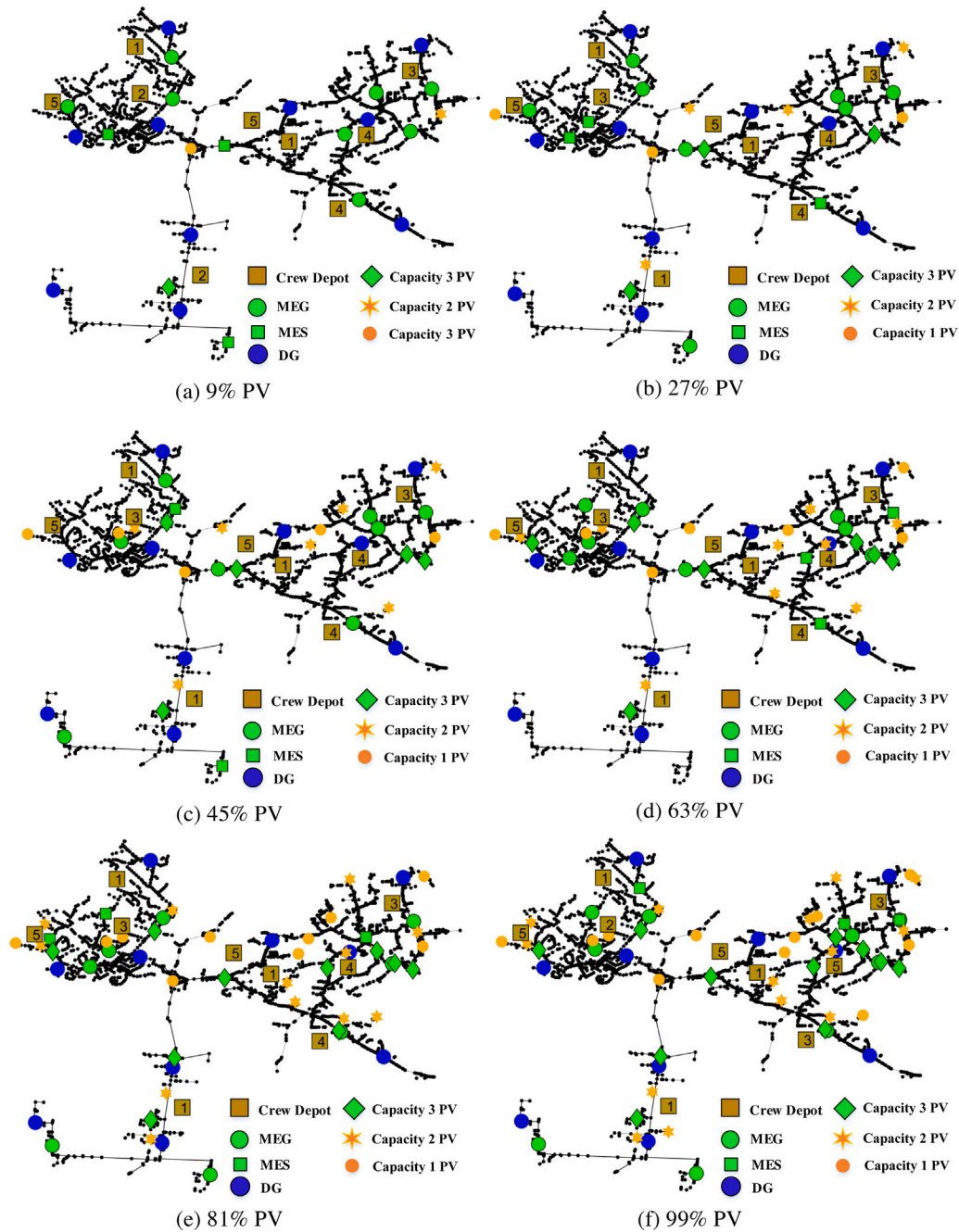
**Fig. 9.** Pre-event resource allocation results with different PV penetration levels.

proposed method, the total restored energy is 291,727.48 kWh and the average outage duration is 11.28 h. Therefore, approximately 20.67% more loads are served by the proposed method and the outage duration decreased by 30.22%.

### 4.2. Impacts of solar PV on system resilience

To show the advantages of the PV systems, the responses of the system with the proposed pre-event preparation method and different PV penetration levels are tested. Three rated capacities of PV systems are considered: (i) Capacity 1 PV, which represents residential PV panels and the rated capacity is assumed to be 6 kW; (ii) Capacity 2 PV, which represents mid-size PV systems and the rated capacity is assumed to be 48 kW; (iii) Capacity 3 PV, which represents large utility PV farm and the rated capacity is assumed to be 2000 kW. Based on the number

of different types of PVs, 6 PV penetration levels are defined as 9%, 27%, 45%, 63%, 81%, and 99%. The number of Capacity 1, 2, and 3 PVs for each PV penetration level is summarized in Table 1. To better collaborate the setting of PV penetration, the number of dispatchable DGs has been changed to 10 and the positions of those DGs have been changed accordingly.

Based on the results of Fig. 9, it can be observed that different PV penetration levels have different allocation results for the flexible resources, including the positions of MEGs, MESs, and the number of repair crews.

Fig. 10 shows the percentage of power served during the event, and after the repair process starts. Tables 2 and 3 compare the amount of load served and average outage duration with different levels of PV penetration.

Based on the results from Fig. 10, Table 2, and Table 3, it can be seen that the penetration of PV contributes to enhancing system
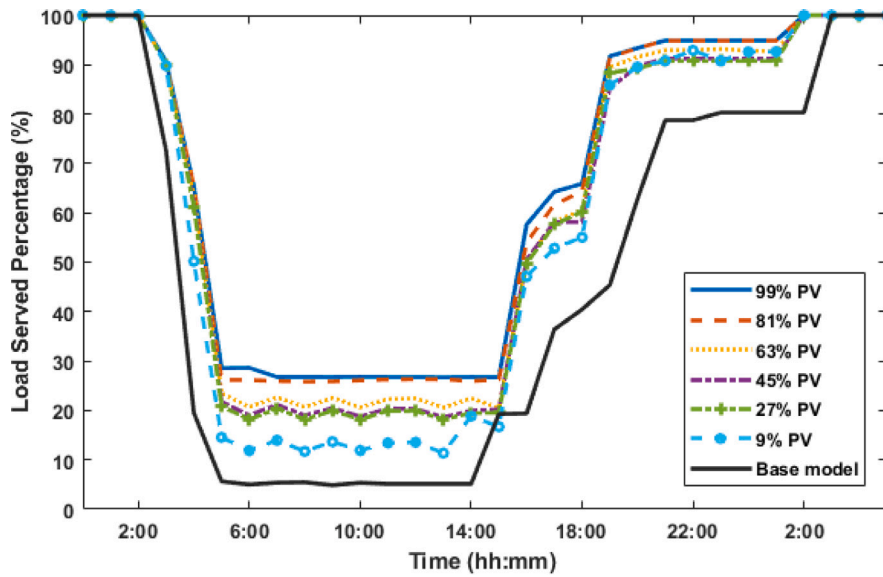
**Fig. 10.** Load served percentage comparison of the proposed model with various PV penetration levels and the base model.

**Table 1**
PV penetration levels and the number of PV systems with different rated capacities.

| PV penetration level | Capacity 1 PV | Capacity 2 PV | Capacity 3 PV |
|---|---|---|---|
| **9%** | 8 | 1 | 1 |
| **27%** | 24 | 4 | 3 |
| **45%** | 40 | 7 | 5 |
| **63%** | 63 | 9 | 7 |
| **81%** | 72 | 12 | 9 |
| **99%** | 88 | 15 | 11 |

**Table 2**
The amount of load served and resilience improvement with different PV penetration levels.

| PV penetration level | Load served (kWh) | Resilience improvement percentage (%) |
|---|---|---|
| **0** | 251,210.72 | – |
| **9%** | 318,668.37 | 26.85 |
| **27%** | 335,525.77 | 33.56 |
| **45%** | 336,710.74 | 34.04 |
| **63%** | 344,588.22 | 37.17 |
| **81%** | 360,668.04 | 43.57 |
| **99%** | 364,785.93 | 45.21 |

**Table 3**
The amount of average outage duration and outage decreased percentage with different levels of PV penetration.

| PV penetration level | Average outage duration (h) | Outage decreased percentage (%) |
|---|---|---|
| **0** | 14.69 | – |
| **9%** | 12.33 | 16.07 |
| **27%** | 11.72 | 20.22 |
| **45%** | 11.65 | 20.69 |
| **63%** | 11.21 | 23.69 |
| **81%** | 10.45 | 28.86 |
| **99%** | 10.12 | 31.11 |

resilience. Approximately 31.13% more loads are served than the base model when the proposed method with 99% PV penetration is used. Also, the average outage duration decreased by 31.12%. However, compared with 81% PV penetration level, the proposed method with 99% PV penetration does not have significant improvement.

## 5. Conclusion

Extreme weather events may severely impact the electric grid infrastructures, causing major damage and faults in the system. This leads to power outages for an extended period. It is up to the electric utility to plan how to prepare for such an event and restore power to the customers after the event. When an extreme weather event hits the distribution system, the damaged network may hinder the physical delivery of mobile resources and repair crews. In addition, without proper preparation, utilities will be overwhelmed with the number of tasks that must be conducted, including assigning tasks to crews, managing crews coming from different areas, and dispatching portable generators to supply critical customers. Therefore, to achieve fast and efficient response, it is critical to pre-position crews, equipment, and other resources before the severe event occurs. In this paper, a two-stage stochastic pre-event preparation and resource allocation method is proposed for upcoming extreme weather events, which enhances the system resilience and enables more efficient post-event restoration. The proposed pre-event method leverages the pre-allocation of mobile resources, fuel resources, and labor resources. By considering different operation modes of distributed PV systems, the proposed model also facilitates the benefits of solar powers in the resilience improvement of distribution grids. According to the case studies, the following observations are found: (i) Compared to the base model without pre-event resource allocation, the proposed pre-event preparation model can serve more loads and reduce the outage duration. (ii) Based on the response of the system with different PV penetration levels, it can be observed that the proposed pre-event preparation model with high PV penetration can further improve system resilience and reduce the outage duration. Therefore, PV systems can play a critical role in improving distribution grid resilience and further promote renewable energy deployment. (iii) By considering the trade-off between solution accuracy and computation efficiency, the result of MRP indicates that the proposed model's solutions with a limited number of scenarios can be very stable and of high quality. The scalability of the proposed pre-event preparation model is verified with a large-scale system. The trade-off between the cost of pre-event resource allocation and the risk associated with damage loss will be considered under upcoming extreme weather events in future work.

### CRediT authorship contribution statement

**Qianzhi Zhang:** Conceptualization, Methodology, Software, Writing - original draft, Validation. **Zhaoyu Wang:** Supervision, Project

administration, Funding acquisition. **Shanshan Ma:** Writing - review & editing, Software, Validation, Methodology. **Anmar Arif:** Writing - review & editing, Software, Validation, Methodology.

### Declaration of competing interest

The authors declare that they have no known competing financial interests or personal relationships that could have appeared to influence the work reported in this paper.

### Acknowledgment

### References

[1] Craig MT, Cohen S, Macknick J, Draxl C, Guerra OJ, Sengupta M, et al. A review of the potential impacts of climate change on bulk power system planning and operations in the United States. Renew Sustain Energy Rev 2018;98:255–67.

[2] Feldpausch-Parker AM, Peterson TR, Stephens JC, Wilson EJ. Smart grid electricity system planning and climate disruptions: A review of climate and energy discourse post-superstorm sandy. Renew Sustain Energy Rev 2018;82:1961–8.

[3] Abdin L, Fang Y, Zio E. A modeling and optimization framework for power systems design with operational flexibility and resilience against extreme heat waves and drought events. Renew Sustain Energy Rev 2019;112:706–19.

[4] Pantrli M, Mancarella P. Influence of extreme weather and climate change on the resilience of power systems: Impacts and possible mitigation strategies. Electr Power Syst Res 2015;127:259–70.

[5] Martin N, Rice J. Power outages, climate events and renewable energy: Reviewing energy storage policy and regulatory options for Australia. Renew Sustain Energy Rev 2021;137:110617.

[6] Salman AM, Li Y, Stewart MG. Evaluating system reliability and targeted hardening strategies of power distribution systems subjected to hurricanes. Reliab Eng Syst Saf 2015;144:319–33.

[7] Campbell RJ, Lowry S. Weather-related power outages and electric system resiliency. Congressional Research Service, Library of Congress Washington, DC; 2012.

[8] Das L, Munikoti S, Natarajan B, Srinivasan B. Measuring smart grid resilience: Methods, challenges and opportunities. Renew Sustain Energy Rev 2020;130:109918.

[9] Molyneaux L, Brown C, Wagner L, Foster J. Measuring resilience in energy systems: Insights from a range of disciplines. Renew Sustain Energy Rev 2016;59:1068–79.

[10] Sharifi A, Yamagata Y. Principles and criteria for assessing urban energy resilience: A literature review. Renew Sustain Energy Rev 2016;60:1654–77.

[11] Emenike SN, Falcone G. A review on energy supply chain resilience through optimization. Renew Sustain Energy Rev 2020;134:110088.

[12] Tari AN, Sepasian MS, Kenari MT. Resilience assessment and improvement of distribution networks against extreme weather events. Int J Power Energy Syst 2021;125:106414.

[13] Executive Office of the President. Economic benefits of increasing electric grid resilience to weather outages. White House Tech. Rep., 2020.

[14] Mishra DK, Ghadi MJ, Azizivahed A, Li L, Zhang J. A review on resilience studies in active distribution systems. Renew Sustain Energy Rev 2021;135:110201.

[15] Ma S. Resilience-Oriented Design and Proactive Preparedness of Electrical Distribution System (Ph.D. thesis), 2020.

[16] Lin Y, Bie Z. Tri-level optimal hardening plan for a resilient distribution system considering reconfiguration and DG islanding. Appl Energy 2018;211:1266–79.

[17] Dehghani NL, Jeddi AB, Shafieezadeh A. Intelligent hurricane resilience enhancement of power distribution systems via deep reinforcement learning. Appl Energy 2021;285:116355.

[18] Zhang G, Zhang F, Zhang X, Wu Q, Meng K. A multi-disaster-scenario distributionally robust planning model for enhancing the resilience of distribution systems. Int J Power Energy Syst 2020;122:106161.

[19] Shahbazi A, Aghaei J, Pirouzi S, Shafie-khah M, Catalao JP. Hybrid stochastic robust optimization model for resilient architecture of distribution networks against extreme weather conditions. Int J Power Energy Syst 2021;126:106576.

[20] Arif A, Wang Z, Wang J, Chen C. Power distribution system outage management with co-optimization of repairs, reconfiguration, and DG dispatch. IEEE Trans Smart Grid 2018;9(5):4109–18.

[21] Mousavizadeh S, haghifam M-R, Shariatkhah M-H. A linear two-stage method for resiliency analysis in distribution systems considering renewable energy and demand response resources. Appl Energy 2018;211:443–60.

[22] Amirioun M, Aminifar F, Lesani H, Shahidehpour M. Metrics and quantitative framework for assessing microgrid resilience against wind storms. Int J Power Energy Syst 2019;104:716–23.

[23] Zhang Q, Ma Z, Zhu Y, Wang Z. A two-level simulation-assisted sequential distribution system restoration model with frequency dynamics constraints. IEEE Trans Smart Grid 2021;12(5):3835–46.

[24] Gholami A, Shekari T, Grijalva S. Proactive management of microgrids for resiliency enhancement: An adaptive robust approach. IEEE Trans Sustain Energy 2019;10(1):470–80.

[25] Wang C, Hou Y, Qiu F, Lei S, Liu K. Resilience enhancement with sequentially proactive operation strategies. IEEE Trans Power Syst 2017;32(4):2847–57.

[26] Panteli M, Mancarella P, Trakas D, Kyriakides E, Hatziargyriou N. Metrics and quantification of operational and infrastructure resilience in power systems. IEEE Trans Power Syst 2017;32(6):4732–42.

[27] Wang S, Sarker B, Mann L, Triantaphyllou E. Resource planning and a depot location for electric power restoration. European J Oper Res 2004;155(1):22–43.

[28] Arif A, Wang Z, Chen C, Chen B. A stochastic multi-commodity logistic model for disaster preparation in distribution systems. IEEE Trans Smart Grid 2020;11(1):565–76.

[29] Taheri B, Safdarian A, Moeini-Aghtaie M, Lehtonen M. Enhancing resilience level of power distribution systems using proactive operational actions. IEEE Access 2019;7:137378–89.

[30] Lei S, Wang J, Chen C, Hou Y. Mobile emergency generator pre-positioning and real-time allocation for resilient response to natural disasters. IEEE Trans Smart Grid 2018;9(3):2030–41.

[31] Lei S, Chen C, Zhou H, Hou Y. Routing and scheduling of mobile power sources for distribution system resilience enhancement. IEEE Trans Smart Grid 2019;10(5):5650–62.

[32] Kim J, Dvorkin Y. Enhancing distribution system resilience with mobile energy storage and microgrids. IEEE Trans Smart Grid 2019;10(5):4996–5006.

[33] Samara S, Shaaban M, Osman A. Optimal management of mobile energy generation and storage systems. IEEE Access 2020;8:203890–900.

[34] Okoye CO, Taylan O, Baker DK. Solar energy potentials in strategically located cities in Nigeria: Review, resource assessment and PV system design. Renew Sustain Energy Rev 2016;55:550–66.

[35] Emmanuel M, Rayudu R. Evolution of dispatchable photovoltaic system integration with the electric power network for smart grid applications: A review. Renew Sustain Energy Rev 2017;67:207–24.

[36] Ranaweera I, Midtgard O-M. Optimization of operational cost for a grid-supporting PV system with battery storage. Renew Energy 2016;88:262–72.

[37] Belding S, Walker A, Watson A. Will solar panels help when the power goes out?. National renewable energy tech. rep., 2020.

[38] Schmitz WI, Schmitz M, Canha LN, Garcia VJ. Proactive home energy storage management system to severe weather scenarios. Appl Energy 2020;279:115797.

[39] Rosales-Asensio E, de Simon-Martin M, Rosales A-E, Comenar-Santos A. Solar-plus-storage benefits for end-users placed at radial and meshed grids: An economic and resiliency analysis. Int J Power Energy Syst 2021;128:106675.

[40] Zhang C, Wei Y-L, Cao P-F, Lin M-C. Energy storage system: Current studies on batteries and power condition system. Renew Sustain Energy Rev, Early Access.

[41] Rockafellar RT, Wets RJ-B. Scenarios and policy aggregation in optimization under uncertainty. Math Oper Res 1991;16(1):119–47.

[42] Watson J-P, Woodruff DL. Progressive hedging innovations for a class of stochastic mixed-integer resource allocation problems. Comput Manag Sci 2011;8(4):355–70.

[43] Arif A, Wang Z, Chen C, Wang J. Repair and resource scheduling in unbalanced distribution systems using neighborhood search. IEEE Trans Smart Grid 2020;11(1):673–85.

[44] Ma S, Chen B, Wang Z. Resilience enhancement strategy for distribution systems under extreme weather events. IEEE Trans Smart Grid 2018;9(2):1442–51.

[45] Ma S, Li S, Wang Z, Qiu F. Resilience-oriented design of distribution systems. IEEE Trans Power Syst 2019;34(4):2880–91.

[46] Chen B, Chen C, Wang J, Butler-Purry K. Sequential service restoration for unbalanced distribution systems and microgrids. IEEE Trans Power Syst 2018;33(2):1507–20.

[47] Melhem F, Grunder O, Hammoudan Z, Moubayed N. Energy management in electrical smart grid environment using robust optimization algorithm. IEEE Trans Ind Appl 2018;54(3):2714–26.

[48] Zhang Q, Dehghanpour K, Wang Z. Distributed CVR in unbalanced distribution systems with PV penetration. IEEE Trans Smart Grid 2019;10(5):5308–19.

[49] Ma S, Su L, Wang Z, Qiu F, Guo G. Resilience enhancement of distribution grids against extreme weather events. IEEE Trans Power Syst 2018;33(5):4842–53.

[50] EPRI. OPENDSS test circuits. 2019, URL https://sourceforge.net/p/electricdss/discussion/beginners.html.

[51] Arritt R, Dugan R. The IEEE 8500-node test feeder. In: IEEE PES T&D Conference. 2010, p. 1–6.

[52] Hart WE, Laird CD, Watson J-P, Woodruff DL, Hackebeil GA, Nicholson BL, et al. Pyomo-optimization modeling in Python, vol. 67. Springer; 2017.